Chemical composition of monsoon bulk precipitation in the Salalah area, Oman

Nils Michelsen[a], Jan Friesen[b], Gerhard Strauch[c], Zulaina Mohammed Al-Balushi[d], Ali Bakhit Ali Bait Said[e], Hajar Al Balushi[f], Mark Schmidt[g], Thomas Müller[c,g]

[a] Institute of Applied Geosciences, Technical University of Darmstadt, Schnittspahnstr. 9, 64287 Darmstadt, Germany

[b] Environmental and Biotechnology Centre, UFZ Helmholtz Centre for Environmental Research, Theodor-Lieser-Str. 4, 06120 Halle, Germany

[c] Department of Hydrogeology, UFZ Helmholtz Centre for Environmental Research, Permoserstr. 15, 04318 Leipzig, Germany

[d] Department of Applied Geosciences, German University of Technology in Oman, PO Box 1816, Athaibah, PC 130, Muscat, Sultanate of Oman

[e] Ministry of Agriculture, Fisheries and Water Resources, PO Box 467, Muscat, PC 100, Sultanate of Oman

[f] Ministry of Higher Education, Research & Innovation (The Research Council), PO Box 82, Ruwi, PC 112, Sultanate of Oman

[g] GEOMAR Helmholtz Centre for Ocean Research Kiel, Wischhofstraße 1-3, 24148 Kiel, Germany

Corresponding author: Thomas Müller; thmueller@geomar.de

Chemical Geology, Volume 635, 121621

https://doi.org/10.1016/j.chemgeo.2023.121621

Abstract

Precipitation chemistry data provide important information for environmental studies on large-scale element cycling and anthropogenic impacts on our atmosphere, but also for hydrochemical models and groundwater recharge estimations via the Chloride Mass Balance method. Such recharge data play a crucial role in groundwater management, particularly in (semi-)arid areas. Unfortunately, precipitation analyses are often scarce in such regions. This also applies to the Arabian Peninsula, including southern Oman. To overcome this lack of rain chemistry data, we developed a strategy for automatic weekly bulk precipitation sampling, using recently designed automatic rainwater samplers. The integral samples were gathered along an elevation gradient from the Salalah coast to the Dhofar mountains during the Indian Ocean Monsoon seasons 2017 and 2018.

Our major ion analyses of the rainwater samples revealed considerable temporal and spatial heterogeneity, in terms of ion proportions and absolute concentrations. Samples from the coast were relatively salty (EC mostly >3000 µS cm^{-1}) and rich in Na^+ and Cl^-, reflecting small rain amounts and a sea spray effect. Further inland, solute concentrations were lower, partly due to more precipitation, and ions such as Ca^{2+} and SO_4^{2-} gained importance, probably due to calcite and gypsum dust. This pattern reflects the interplay between solute availability (influenced by regional geology, wind direction at different altitudes, and wind speed) and precipitation amounts. Cl^-/Br^- ratios were fairly uniform and scattered around the seawater value. Combining ion concentrations and rain amounts yielded bulk depositions that showed an erratic pattern along the elevation gradient, i.e., depositions did not decrease steadily in inland direction, as one may assume. This suggests that the occasionally reported approach of collecting a few opportunistic grab samples at a single site is unlikely to yield data that are representative for a larger coastal study area.

Key words: rain, precipitation chemistry, dry deposition, Indian Ocean Monsoon, Khareef, Dhofar

1. Introduction

Precipitation chemistry data are crucial for our understanding of local and global atmospheric element cycling and for an assessment of corresponding anthropogenic impacts (Ahmed et al., 1990; Decina et al., 2019; Liotta et al., 2021; Riechelmann et al., 2022; Tso et al., 2022; Vet et al., 2014). Moreover, precipitation is the initial solvent or "titrant" in hydrogeochemical systems (Edmunds, 2010) and its major ion concentrations are required as input data for hydrochemical models (Christofi et al., 2020; Paukert et al., 2012; Solder and Jurgens, 2020).

While precipitation chemistry monitoring networks are established in some parts of the world, several regions lack adequate data (Vet et al., 2014). One example is the Arabian Peninsula, where isolated studies have been conducted, using different approaches (Ahmed et al., 1990; Alabdula'aly and Khan, 2000; Matter et al., 2005; Michelsen et al., 2015; Müller et al., 2020; Schemenauer and Cereceda, 1992; Strauch et al., 2014; Weyhenmeyer, 2000; Wood et al., 2010; see Table S1, Fig. S1), but overall data coverage is still poor. This data scarcity does not only affect atmospheric research in the region, but also hampers the application of a number of methods to study groundwater. Examples include 1) the Chloride Mass Balance method, 2) the use of the ion ratio Cl^-/Br^- in hydrochemical studies, and 3) hydrochemical models.

Chloride mass balance calculations are a versatile tool (Cartwright et al., 2013, 2017; Keppel et al., 2012). Arguably, the most popular application is the estimation of groundwater recharge, based on the atmospheric deposition of chloride and its concentration in groundwater. Due to the simplicity of the method, it is generally popular in (semi-)arid areas and can be a powerful tool to assess groundwater replenishment (Scanlon et al., 2002) – if the required long-term data on atmospheric chloride are available (Scanlon et al., 2006). Yet, due to data scarcity, Imes and Wood (2007) used the mean chloride concentration of only four rain events (4.6 mg L^{-1}) in their study in the United Arab Emirates. Similarly, Abdalla et al. (2018) considered an average chloride value from seven rain samples (12.6 mg L^{-1}) for their study area in Oman. In the latter case, it is noteworthy that their study area ranged from the coast to the North Oman Mountains (distance approx. 70 km; elevation difference >1,500 m; sampling point elevation difference up to >600 m), which raises the question, if one can indeed assume the chloride concentration in rain to be homogenous in such a setting (see also Weyhenmeyer et al., 2002). A number of studies report a significant spatial variability of precipitation chemistry at the coast (Blew and Edmonds, 1995; Bresciani et al., 2014; Guan et al., 2010; Ladouche et al., 2009; Sanz et al., 2002), but the corresponding coastal transects are mostly located in more humid regions such as the United States, Southern Australia, France, or Spain. Data on this phenomenon in arid areas are still scarce.

Apart from the conservative ion Cl^-, the ion ratio Cl^-/Br^- has become an invaluable tracer in groundwater studies (Cartwright et al., 2006; Davis et al., 1998), also on the Arabian Peninsula. While applications of this tool are abundant (Askri et al., 2016; Hussain et al., 2020; Macumber et al., 1998), data on Cl^-/Br^- in precipitation, representing an important end-member, are rare or even non-existent in this part of the world.

Precipitation chemistry data are also helpful for hydrochemical models. Such thermodynamic calculations are, for example, performed in the context of serpentinization of peridotites in Oman. While Paukert et al. (2012) were able to retrieve data on seven Omani rain samples from an unpublished PhD thesis (Weyhenmeyer, 2000), Leong et al. (2021) utilized a global average rainwater as input fluid for their model (cf. Carroll, 1962), presumably because of scarcity of local data.

The Salalah area in Southern Oman is no exception in this respect, but here the scarcity of published rain chemistry data is somewhat surprising. Every summer, the area experiences monsoon rains that replenish the local groundwater resources (Clark et al., 1987; Strauch et al., 2014), forming the backbone of the area's water supply. Even recurring calls for rainwater harvesting schemes (i.e., direct use of rainwater; Abdul-Wahab et al., 2007, 2010) did not trigger comprehensive investigations of the monsoon chemistry. To our knowledge, only two published studies are available and both have a snapshot character. Schemenauer and Cereceda (1992) analyzed seven cloudwater samples from five days between 22 and 30 July 1990 and Strauch et al. (2014) investigated fog and rain samples during a four-day period from 17 to 20 August 2009.

Here, we extend this limited data set by analyzing the entire monsoon seasons of 2017 and 2018 in the Salalah area. Inspired by investigations of coastal transects in more humid regions (Blew and Edmonds, 1995; Guan et al., 2010; Ladouche et al., 2009), the samples were gathered along a 28 km long elevation gradient from the coast to the Dhofar mountains (880 m a.sl.). Yet, unlike many other studies, we used automatic samplers, which allowed us to obtain weekly (time-synchronized) composite samples. The obtained data hence enable an evaluation of 1) temporal dynamics within the monsoon seasons, 2) spatial differences in chemical fingerprints, and 3) underlying mechanisms. To complement the chemical data and to aid interpretation, also modeled air mass back-trajectories are considered.

2. Study area

Salalah is Oman's third-largest city and the capital of the Dhofar governorate. The city's warm, semi-arid climate is characterized by a mean annual air temperature of 26°C with a correspondingly high potential evaporation of about 1700 mm a^{-1} (Shammas and Jacks, 2007). Precipitation mostly occurs in the form of low-intensity rain and drizzle (<10 mm d^{-1}) during the annual Indian Ocean Monsoon

(locally called *khareef*) between mid-June and mid-September (Fig. S2). During this time, southerly winds from the Arabian Sea push moist air masses against the Dhofar mountain range north of Salalah (900-1300 m a.s.l.; Fig. 1, Fig. S3) where they are trapped by a thermal inversion layer (Abdul-Wahab, 2003; Schemenauer and Cereceda, 1992). Occasionally, cyclones contribute precipitation (every 2-6 years, Friesen et al. 2018). Annual precipitation amounts account for roughly 100 mm at the coast and 250 mm at the mountain crest and most of this rain falls during the monsoon (55 and 220 mm, respectively; Hildebrandt et al. 2007).

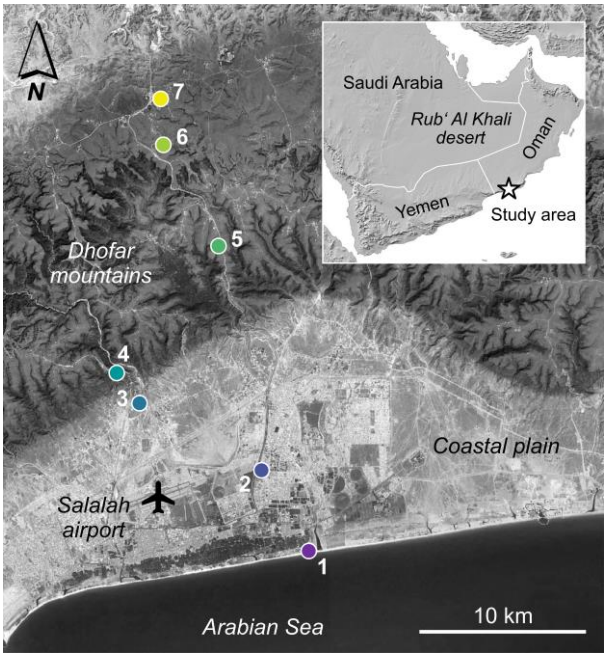

Fig. 1. Map showing the Salalah coastal plain and the adjacent Dhofar mountain range. The area north of the dashed line is dominated by limestones. Colored points represent monitoring stations (see also Table 1; satellite image: Google Earth Pro).

The coastal plain surrounding Salalah shows a length of approx. 60 km and a maximum width of about 15 km (Friesen et al., 2018). It is dominated by Quaternary deposits (mostly sand and gravel) and Pliocene conglomerates towards the mountains. The Dhofar mountain range is mainly build up by Paleocene to Early Eocene limestones of the Umm Er Radhuma Formation (Fig. 1). Further inland, Eocene rocks of the Rus and Dammam Formations (mainly limestone, dolomite, gypsum) are exposed (Ministry of Petroleum and Minerals, 1998).

3. Methods

Precipitation samples were collected at several sites along an elevation gradient from the coast to the mountains (Fig. 1). Due to logistical reasons, monitoring station availability changed slightly between 2017 and 2018 (Table 1).

Table 1. Overview of monitoring stations, including covered years.

ID	Name	Elevation [m a.s.l.]	Distance to sea [km]	Coordinates	2017	2018
7	Qairoon Hairiti	880	28	17°15'9.9"N, 54°5'20.8"E	X	-
6	Gogub	700	25	17°13'42.2"N, 54°5'26.2"E	X	X
5	Rakbeet	510	19	17°10'27.4"N, 54°7'16.4"E	X	X
4	Ittin	330	12	17°6'24.60"N, 54°3'52.6"E	X	X
3	Garsis	93	10	17°5'25.6"N, 54°4'37.5"E	X	X
2	Saadah	30	5	17°3'16.6"N, 54°8'42.9"E	-	X
1	Dahariz	5	0.1	17°0'41.2"N, 54°10'17.9"E	X	X

At each station, a custom-made automatic rain sampler (Michelsen et al., 2019) was installed prior to the monsoon season (17 June 2017 and 23 June 2018). The samplers consist of a funnel leading to a distribution unit to which up to 18 HDPE bottles are connected. Upon installation, the distribution unit was programmed to change the connected bottles in seven-day intervals to obtain weekly (time-synchronized) composite samples. As the funnel is continuously exposed, the sampler acts as a bulk collector, i.e., also dry deposition is collected, if it is flushed down by precipitation. A combination of design features efficiently reduces post-sampling evaporation (lab experiments; see Michelsen et al., 2019) and field controls (*sensu* Michelsen et al., 2018), i.e., weighed pre-filled bottles included in the sampler, suggest maximum mass losses of 0.8 % over the monsoon period. Thus, we conservatively estimate that losses from the actual sampling bottles could be on the order of a few percent or less, and hence within analytical precision (see below).

Shortly after the end of the monsoon season (mid to end of September), the samples were retrieved and rain amounts were determined gravimetrically with a portable scale (EMB 2000-2 by KERN, Balingen, Germany). Electrical conductivity (EC) and pH value were measured with a handheld unit (Multi 3430 by WTW, Weilheim, Germany). If collected water amounts permitted, alkalinity was determined by titration with sulfuric acid (AL-DT alkalinity test kit by HACH, Düsseldorf, Germany) and converted into bicarbonate concentrations. Samples were filtered (0.45 µm) and shipped to the laboratory.

In 2017, chemical analyses were performed at the UFZ Helmholtz Centre for Environmental Research (Leipzig, Germany). Cations were measured by Inductively Coupled Plasma-Optical Emission

Spectroscopy (ICP-OES; ARCOS by SPECTRO Analytical Instruments, Kleve, Germany), SO_4^{2-} and Cl^- were determined by Ion Chromatography (IC; ICS-2000 by Thermo Fisher Scientific, Waltham, MA, USA), and NO_3^- as well as NO_2^- were analyzed photometrically (Gallery Plus by Thermo Fisher Scientific, Waltham, MA, USA). The precision for these parameters is typically better than ±5 % (relative standard deviation). Samples gathered in 2018 were analyzed for all ions with an IC system (882 Compact IC plus by Metrohm, Herisau, Switzerland) at the Institute for Applied Geosciences of the Technical University of Darmstadt (Germany). Here, the precision for the targeted ions is typically better than ±3 %.

Plausibility checks comprised the calculation of charge balance errors and comparison of EC and ion concentration sums (Table S3). Charge balance errors are typically smaller than ±5 %, although a few exceptions are noted. In case of samples with small volumes (preventing alkalinity titration), no error was calculated, but bicarbonate concentrations were estimated from the charge balance (assuming an error of 0 %). Several samples stood out due to elevated PO_4^{3-} concentrations (up to 3.9 mg L^{-1}). As all concerned samples show high NH_4^+ values (up to 40 mg L^{-1}), we suspect contamination by bird droppings (Asman et al., 1982) – despite bird deterrent spikes on the collection funnels. In case of Station 6, elevated NH_4^+ concentrations may also be related to emissions from a nearby cattle farm (Weijers and Vugts, 1990). Hence, no further attempt is made to interpret PO_4^{3-} or N species, and emphasis is placed on the remaining parameters.

Enrichment factors for individual ions relative to bulk seawater (EF) were calculated as follows (Duce et al., 1975):

$$EF = (X/Na^+)_{sample} / (X/Na^+)_{sea} \quad (1)$$

where X is the concentration of the ion of interest. Na^+ is commonly used as reference ion, as it is often assumed to originate exclusively from seawater (droplets or sea spray-derived particles). While some lithogenic Na-bearing dust *may* be present (e.g., halite), the bulk of the Na^+ likely represents a marine input in a coastal setting. Corresponding seawater values were taken from Appelo and Postma (2004).

To constrain solute sources, air mass back-trajectories were calculated with the HYbrid Single-Particle Lagrangian Integrated Trajectory model (HYSPLIT; 48 h trajectories; Stein et al., 2015; Rolph et al., 2017), using the GDAS 0.5° meteorology data set. Salalah airport was chosen as end point (17°2'39.89"N, 54°5'3.46"E; Fig. 1). Back-trajectories were calculated every 12 h (12:00 and 00:00 local time) for air masses reaching two altitudes above the airport – 300 and 1500 m above ground. The first value represents monsoon-related clouds and reflects the mean cloud base altitude during the monsoon (Fig. S3d; see also Schemenauer and Cereceda, 1992). The latter value is representative for the conditions above the thermal inversion layer (see Abdul-Wahab, 2003).

4. Results

4.1 Chemical composition of bulk precipitation

The hydrochemical data are presented in Table S3, along with the corresponding weekly precipitation amounts, ranging from 0 to 77 mm. The maximum was recorded at Station 4 (Ittin, at 330 m a.s.l.).

The pH values range from 4.30 to 7.94, with a precipitation-weighted mean of 6.86, which is higher than the pH of rain in equilibrium with atmospheric CO_2 (5.7 at 25°C; e.g., Carroll, 1962). The EC values scatter between 63 and 26900 µS cm^{-1} and the weighted mean accounts for 295 µS cm^{-1}. Due to this high variability, a station-specific analysis considering precipitation amounts is required (Fig. 2).

Fig. 2 illustrates that the highest EC values were recorded for the coastal Station 1 (at 5 m a.s.l.). Here, values of several thousand µS cm^{-1} are common and also the above-mentioned maximum value was encountered at this site. Stations at higher elevations (further inland) show lower ECs, usually a few hundred µS cm^{-1} or less.

The figure also reveals that higher ECs often occur in weeks with small rain amounts and vice versa. Consequently, temporal aspects become apparent as well, particularly in 2017. Here, Stations 3-7 exhibit weak rains and correspondingly high EC values in the first monsoon week (similar effect at the end of the monsoon). Yet, we do not see an elevated EC in the initial samples gathered in 2018.

Apart from precipitation and EC values, Fig. 2 incorporates chemical composition data – in a simplified way, harnessing the $Na^+/(Na^+ + Ca^{2+})$ ratio. While at the lowest Stations 1-3, ratios >0.5 prevail (Na^+ dominance), Stations 4-6, located farther away from the sea and at higher elevations, mostly show ratios of around 0.5 (balanced) or higher (Ca^{2+} dominance). Exceptions are noted for the first samples that often exhibit a Na^+ predominance. The figure also exhibits temporal developments with increasing Ca^{2+} importance (e.g., Stations 3-6).

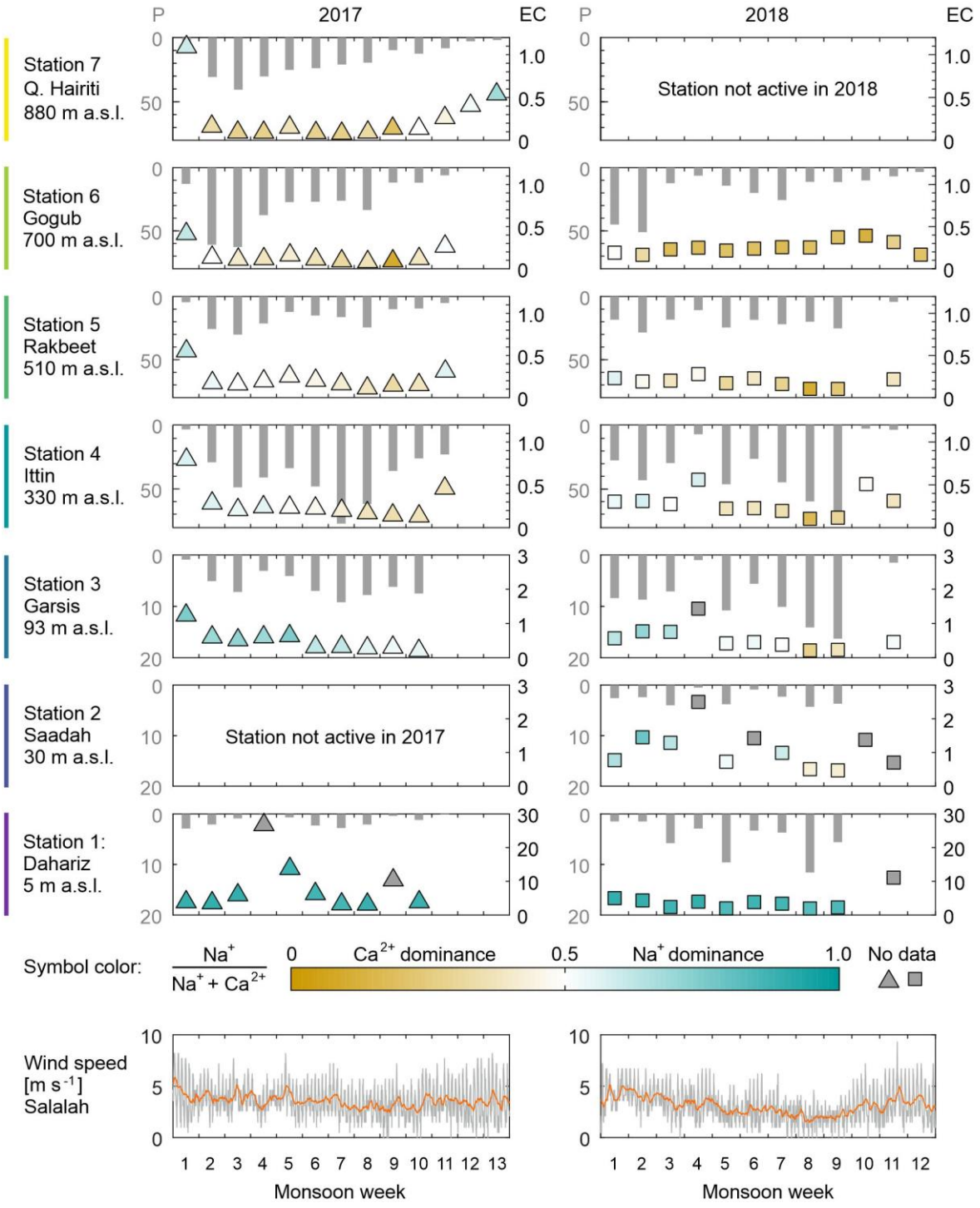

Fig. 2. Development of precipitation amounts P [mm], EC values [mS cm^{-1}], and ion ratios (on a meq basis) during the monsoon seasons 2017 (left) and 2018 (right). Note the partly differing scales. For comparison, wind speeds from Salalah airport are included (accessed via IEM, 2021; see also Fig. S3). In 2017, the first monsoon week starts on 24 June and in 2018 on 30 June.

Aiming at a better understanding of involved solute sources, a set of ion scatter plots was generated (Fig. 3). When plotting Cl^- against Na^+ (Fig. 3a), a large concentration spread becomes apparent (Cl^-: 4-

4340 mg L^{-1}; Na^+: 2-2360 mg L^{-1}). All points fall on or near the line representing seawater dilution and the coastal Station 1 shows the highest concentrations of both ions (Cl^-: 378-4340 mg L^{-1}; Na^+: 209-2360 mg L^{-1}).

Cl^-/Br^- mass ratios (Fig. 3b) range from 120 to 417 and thus show some scatter, but most points fall relatively close to the seawater line representing a ratio of 289 (for comparison: Cl^-/Br^-_{molar}=655), especially at higher Na^+ concentrations. The precipitation-weighted mean ratio accounts for 299.

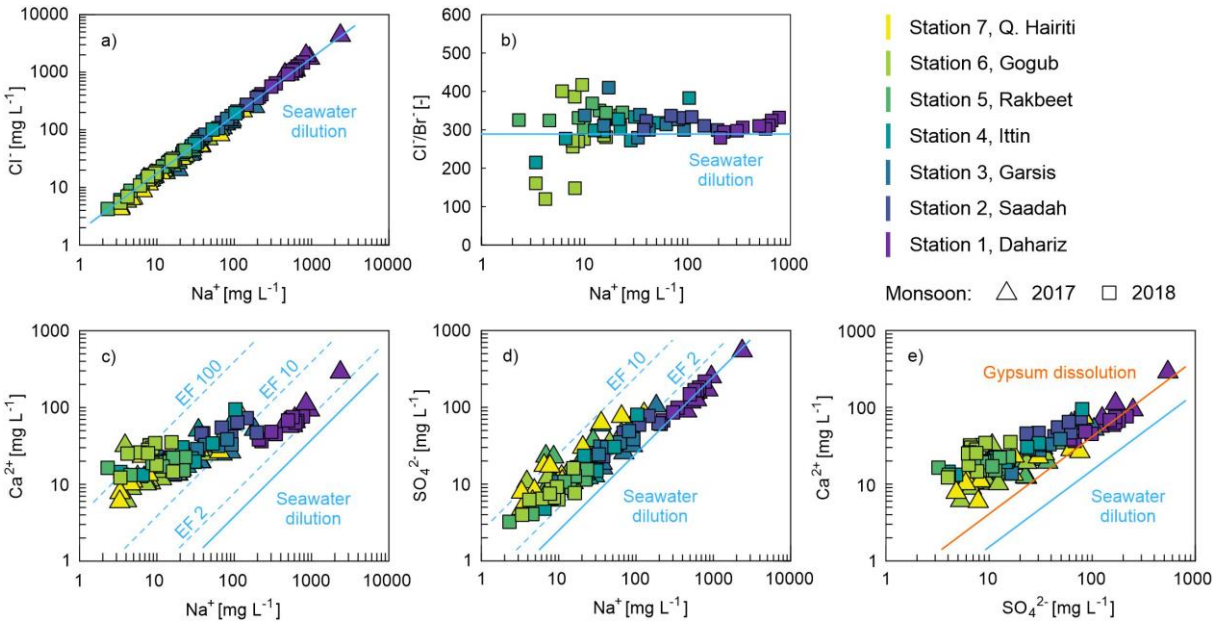

Fig. 3. Scatter plots for selected ions. Data for the construction of the seawater dilution lines are taken from Appelo and Postma (2004). In selected plots, exemplary enrichment factors (EF) are shown. In e), a line representing gypsum (or anhydrite) dissolution was included.

In the Ca^{2+} vs. Na^+ plot (Fig. 3c), all points lie above the seawater dilution line, i.e., the samples contain more Ca^{2+} than one would expect based on the corresponding Na^+ concentration and an assumed ion ratio resembling that of seawater (Ca^{2+} excess). The data also show a SO_4^{2-} excess with respect to seawater, especially for the inland stations at higher elevations (Fig. 3d). The Ca^{2+} vs. SO_4^{2-} plot (Fig. 3e) indicates a Ca^{2+} excess with respect to gypsum, i.e., the ions do not balance each other out (also note the differing EFs in Fig. 3c and 3d).

While these scatter plots focus on ion ratios, absolute concentrations also deserve a closer look, particularly because they are not only governed by salt availability, but apparently also by precipitation amounts (see also Fig. 2). Hence, dedicated plots are presented for two selected ions, Na^+ and Ca^{2+} (Fig. 4). Both charts indeed reveal a dilution effect, i.e., lower concentrations are observed for samples

associated with more rain. Interestingly, the composite samples representing Cyclone Mekunu (Müller et al., 2020; partly matching stations) fit into this picture as well. Moreover, an appreciable offset is observed for the Na^+ data from Station 1 (Fig. 4a).

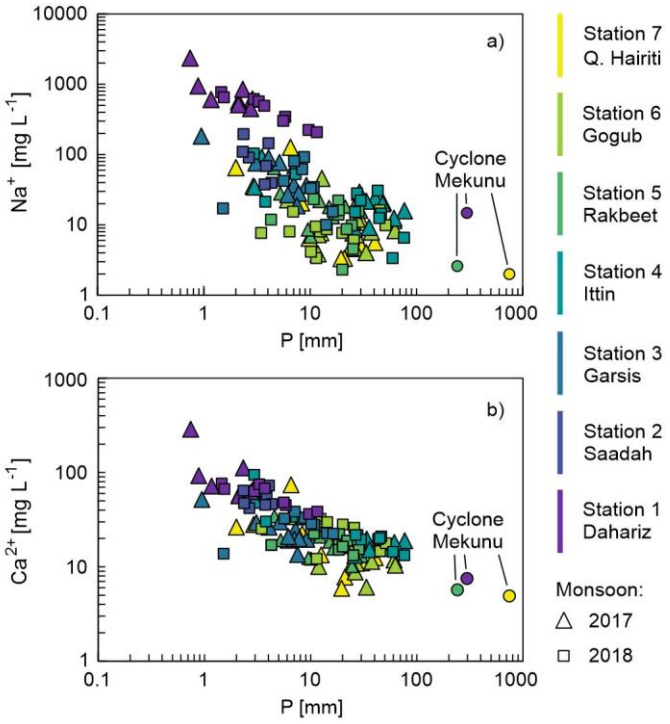

Fig. 4. Scatter plots showing the relation of selected ions with the precipitation amount P. For comparison, composite samples from Cyclone Mekunu (Müller et al., 2020; circles) were included.

4.2 Bulk deposition

The above-mentioned patterns result from the interplay between the availability of solutes and of water for dissolution, and in turn call for an analysis of spatial differences in bulk depositional flux. Thus, the apparent total deposition over the entire monsoon seasons 2017 and 2018 was calculated for each station with the available data (Fig. 5; see also Fig. S4).

The chart again demonstrates the differing hydrochemical characters of the stations. The cation spectrum of the coastal Station 1 is dominated by Na^+ (see also Fig. 2 and 3). In contrast to the inland stations, Ca^{2+} and Mg^{2+} show comparable mass contributions. Among the anions, Cl^- prevails. Further inland, Ca^{2+} contributions increase and Mg^{2+}, Na^+, and Cl^- become less important.

The total depositions do not exhibit a steady decrease along the elevation gradient, as one may expect. They show a spatially erratic pattern, which also differs between the two years. The high bulk depositions at Station 1 of about 37 g m^{-2} (2017) and 58 g m^{-2} (2018) are not too surprising (little rain,

but very high ion concentrations). However, the remarkable values of 54 g m^{-2} (2017) and 56 g m^{-2} (2018) determined for Station 4 (distance to coast 12 km) do stand out. Accordingly, also individual ions exhibit fairly large spreads. In terms of Cl^-, for instance, Station 1 shows deposition rates of 20.4 and 30.0 g m^{-2} in 2017 and 2018, respectively, which are roughly 5 and 7.5 times higher than at the highest stations.

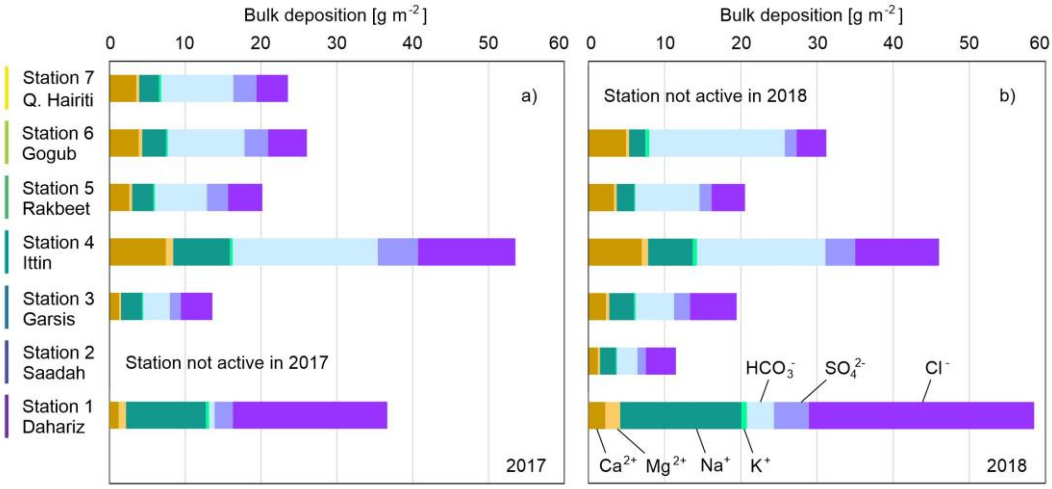

Fig. 5. Apparent major ion depositions for the monsoon seasons 2017 (left) and 2018 (right).

5. Discussion

5.1 Chemical composition of bulk precipitation

The highest EC values, often several thousand µS cm^{-1}, were encountered at the coastal Station 1 (Fig. 2), and inland stations at higher elevations show much lower values. Hence, the station location (distance to sea, elevation) appears to play a role and a sea spray effect seems likely.

Additionally, we found that higher ECs predominantly occur in weeks with small rain amounts (and vice versa; Fig. 2). Elevated EC values were also recorded for the first monsoon week in 2017. These were associated with small rain amounts, but they are likely not the only reason for these initial high ECs. Further reasons are probably 1) the slightly higher wind speeds at this time (Fig. 2), facilitating sea spray generation and inland transport, and 2) that the first rains after a long dry period cause a washout of atmospheric dust. Moreover, it is worth mentioning that 3) the first sampling bottle was found empty at all stations. This implies that dry deposition may have accumulated on the funnel during the first week of exposure (17-24 June 2017), but only entered the first sample (second bottle) in the following week. In 2018, however, the first monsoon week showed no elevated ECs. While also in this season the first bottle remained empty at all stations (like in 2017), the first actual monsoon week

showed fairly high rain amounts. Further, Cyclone Mekunu had hit the area at the end of May 2018, about a month before the monsoon (Fig. S3c). The associated rains, partly exceeding 600 mm within a few days (Müller et al., 2020), probably caused an efficient washout, and the increased soil moisture in the region (incl. parts of the Rub' Al Khali desert; Bürgi and Lohman, 2021) may have hampered subsequent mobilization of particles by wind to some extent.

The higher Na^+ proportions observed at the lower stations are in line with the above-mentioned sea spray effect. The mentioned temporal evolution with an increasing Ca^{2+} role may be related to slightly decreasing wind speeds (Fig. 2), implying that gradually less sea spray is generated and transported inland.

The scatter plots (Fig. 3) illustrate an appreciable concentration spread. Individual Cl^- values, for instance, scatter between 4 and 4340 mg L^{-1}, covering orders of magnitude. As a part of this variability reflects weekly fluctuations, we also calculated precipitation-weighted Cl^- means for the entire monsoon seasons. In the 2017 monsoon, the values range from 16 mg L^{-1} (Station 6) to 1360 mg L^{-1} (Station 1), and in the 2018 monsoon, they fall between 18 mg L^{-1} (Station 6) to 650 mg L^{-1} (Station 1; see Table S2). Hence, the mean Cl^- concentrations at the "saltiest" station are 85 times (2017) and 36 times (2018) higher than those at the "freshest" station in the mountains. Although a comparison with other studies is hampered by differing study designs (distances, elevations, temporal scales), our generally high Cl^- concentrations and their spatial heterogeneities seem remarkable. Mean concentrations reported for other coastal areas (USA, Australia, France, Spain) are usually lower and less variable (Blew and Edmonds, 1995; Bresciani et al., 2014; Guan et al., 2010; Ladouche et al., 2009; Sanz et al., 2002; Table S2). Ladouche et al. (2014), for example, report a mean of about 3.5 mg L^{-1} for a station 50 km inland (at 583 m a.s.l.; Southern France) and 20.3 mg L^{-1} for their coastal site (3 km inland).

Apart from the above-mentioned scatter, the Cl^- vs. Na^+ plot (Fig. 3a) shows a good match of the data with the seawater dilution line and hence confirms the sea spray effect, particularly for the lower stations that feature the highest concentrations. While Müller et al. (2020) emphasized the importance of sea spray for the study area in a cyclone context, it seems to play a role in the monsoon season as well. Here, also the elevated significant wave heights during the monsoon – typically 2-2.5 m near the coast and around 3 m offshore (Anoop et al., 2015; Bruno et al., 2020) – are noteworthy.

The sea spray effect becomes apparent in the Cl^-/Br^- mass ratios too (Fig. 3b) – most are similar to the seawater value. Although some deviations are noted for higher stations (especially Station 6), the overall precipitation-weighted mean ratio accounts for 299, which is close to the seawater value of 289.

However, the Ca^{2+} excesses (Fig. 3c) suggest that not all ions originate from sea spray. While Ca^{2+} enrichment in sea spray aerosol particles has been observed in chamber experiments with natural and artificial seawater (Keene et al., 2007; Salter et al., 2016), the reported enrichment factors are comparatively small (on the order of 1.2, Keene et al., 2007). As our EFs are much greater, particularly at higher elevations (EF partly >100), a lithogenic Ca^{2+} source seems likely (e.g., calcite, dolomite, gypsum). This also (and particularly) applies, if some of the Na^{+} is actually lithogenic, instead of marine as commonly assumed.

Interestingly, many samples also show a SO_4^{2-} excess with respect to seawater (Fig. 3d), especially those from inland stations at higher elevations. Generally, elevated SO_4^{2-} are often associated with anthropogenic SO_x emissions (e.g., Ahmed et al., 1990; Junge and Werby, 1958; Vet et al., 2014), but the encountered enrichments seem too high to be mainly caused by pollution, despite intense traffic during Salalah's monsoon season (Al-Shidi et al., 2020; Charabi et al., 2018). Moreover, oceanic dimethyl sulfide (DMS) emissions may play a role – in general, but particularly in the Arabian Sea with its increased DMS fluxes (Erickson et al., 1990; Wang et al., 2020). Yet, if DMS was the dominant SO_4^{2-} source, we would expect a greater SO_4^{2-} enrichment at the coastal site, compared to the inland stations. Hence, also here we suspect a large contribution by a lithogenic source and in view of the above-mentioned Ca^{2+} excess, atmospheric dust rich in gypsum ($CaSO_4 \cdot 2H_2O$) and/or anhydrite ($CaSO_4$) seems probable. In this context, it is worth mentioning that calcium sulphates are common dust constituents in the region and have been detected in dust samples from western and central Saudi Arabia (Engelbrecht et al., 2017; Pósfai et al., 2013), Kuwait (Khalaf et al., 1985), Qatar (Javed et al., 2017), the United Arab Emirates (Semeniuk et al., 2014), and Northern Oman (Abdul-Wahab et al., 2005; Semeniuk et al., 2014). Further, they have been reported to occur in aerosol samples collected over the Arabian Sea/Indian Ocean (Johansen et al., 1999; Savoie et al., 1987). In the vicinity of the study area, these minerals occur in the Eocene Rus formation, which crops out north of the Dhofar mountains (see Section 2; Ministry of Petroleum and Minerals, 1998). Additionally, salt pans covering large parts of the southeastern Arabian Peninsula (about 36500 km^2; Schulz et al., 2015), for example in the Rub' Al Khali desert, are a potential gypsum source (Abdul-Wahab et al., 2005; Michelsen et al., 2015). However, both sources could only play a role for the present study, if corresponding dust was transported in roughly southern direction, i.e., against the dominating monsoon wind regime. The air mass back-trajectory modeling with HYSPLIT indeed revealed that such winds occur during the monsoon season, but at higher altitudes (see Fig. S5). While the air masses arriving at 300 m above the Salalah plain mostly come from the southwest, those arriving at 1500 m have more variable sources, but many pass over the interior of the Arabian Peninsula. We hence assume that they deliver gypsum and/or anhydrite dust, which then settles into the top of the trapped cloud layer, where it can be incorporated by droplets (see also Schemenauer and Cereceda, 1992).

To examine whether this mechanism can explain the Ca^{2+} and SO_4^{2-} excesses simultaneously, we harness the corresponding scatter plot (Fig. 3e). The Ca^{2+} excess with respect to gypsum demonstrates that the ions do not balance each other out. Hence, an additional Ca^{2+} source is required, apart from gypsum and/or anhydrite. Given that much of the study area is dominated by limestones of the Umm Er Radhuma formation (Paleocene to Eocene; see Section 2, Fig. 1), calcite dust is deemed a likely additional Ca^{2+} source. Due to the neutralizing capacity of calcite dust, this conclusion is also in line with the comparatively high pH values mentioned above.

Due to this lithogenic SO_4^{2-} and Ca^{2+} contribution by gypsum and limestone, we disagree with Schemenauer and Cereceda (1992). In their analysis of seven cloudwater samples from the area, they suggested the Ca^{2+} in precipitation of the Dhofar mountains to be largely of anthropogenic origin. They apparently drew this conclusion based on high enrichment factors with respect to the Earth's *crust* (and seawater), which may be misleading when dealing with a limestone-dominated study area (see also Yigiterhan et al., 2018).

5.2 Bulk deposition

Given the influence by sea spray, the depositional flux at the coastal Station 1 is dominated by Na^+ and Cl^- (Fig. 5). The contributions by Ca^{2+} and Mg^{2+} are similar to each other, which is attributable to the relative Mg^{2+} abundance in seawater.

The total depositions exhibit a somewhat erratic pattern. Especially Station 4 stands out due to its high fluxes. This phenomenon results from a combination of moderate ion concentrations and anomalously high precipitation amounts (see Fig. 2), probably caused by the station's rain-out prone location just above the foot of the Dhofar mountains (at 330 m a.sl.). As a consequence, the Cl^- deposition at Station 4 is about 2-3 times higher than at other inland stations, including Station 3, which is only 2.3 km away, but at 93 m a.s.l..

Overall, these deposition rates, including those for Cl^-, seem rather high. As noted above, direct comparisons with other investigations are not straightforward because of differing study designs. Nevertheless, it is noted that our highest Cl^- deposition values during the monsoon are higher than *annual* fluxes reported elsewhere (Table S2). In turn, our spatial variabilities in Cl^- flux (factors of 5 and 7.5; see Section 4.2) are high, but not extreme (Table S2).

5.3 Limitations

Although our data and interpretations represent a significant extension of previous knowledge on the bulk precipitation chemistry in southern Oman, we emphasize that our results are limited to the

monsoon season (about 3 months). While this season plays an important role for the hydrology of the area, our deposition values do not take into account solute contributions by non-monsoon precipitation (studied by Müller et al., 2020) and dry deposition during the rest of the year. Moreover, we note that our findings for the two studied years differed somewhat (see Fig. 5), suggesting that further monitoring is needed for a more comprehensive picture.

6. Conclusions and Outlook

Our study on the chemical composition of monsoon bulk precipitation along an elevation gradient from the coast to the Dhofar mountains has revealed rather high solute concentrations and depositional fluxes. Moreover, we found considerable temporal and spatial variability, with respect to ion proportions and absolute concentrations.

This variability implies that a collection of opportunistic grab samples at a single site, as occasionally encountered in the literature, is not advisable. Such an approach may yield data that are not representative for larger coastal study areas and could hence impair subsequent hydrochemical models and assessments. Salty coastal groundwater, for instance, may be thought to be entirely caused by seawater intrusion, although local recharge can also contribute significant solute amounts. Moreover, recharge estimations based on the Chloride Mass Balance approach may be affected by ignoring spatial heterogeneities in precipitation chemistry (and amount). In our study, individual Cl^- concentrations cover orders of magnitude (4-4340 mg L^{-1}) and precipitation-weighted means differ greatly between stations, up to factors of 85 and 36 in the 2017 and 2018 monsoons, respectively. Such a variability indicates that even this supposedly easy-to-obtain parameter of the Chloride Mass Balance may not be straightforward to determine in coastal areas.

Our results indicate that the bulk precipitation chemistry is influenced by a complex interplay of several factors. First, the availability of solutes, for example originating from sea spray and the local/regional geology, plays a crucial role. Importantly, this availability is not only a question of distance to the source, but wind directions (at different altitudes) and wind speed matter as well (see also Javed et al., 2017). Second, precipitation amounts have to be considered. High amounts (e.g., triggered by local topography) can cause a dilution effect, but efficient aerosol washout may also result in anomalously high solute deposition. In the present study, this caused an erratic deposition pattern, i.e., fluxes did not decrease steadily along the elevation gradient, as one may expect. This demonstrates that simple interpolations and models, which work well on a large scale (e.g., Alcalá and Custodio, 2008; Davies and Crosbie, 2018; Junge and Werby, 1958), may not do so on smaller scales. While such predictions hence remain challenging, they may be improved by considering local features such as the prevailing geology.

Our data do not only serve generally as a warning against unconsidered extrapolation of rain chemistry in coastal settings, but could also provide reference data for studies in the region. Groundwater quality assessments or serpentinization studies, for example, may benefit from data on the hydrochemistry of infiltrating water (at different distances to the sea), to trace and predict effects of water-rock-interaction. Moreover, groundwater recharge estimations using chloride mass balances may be facilitated. Nevertheless, we note that there were differences between the monsoon seasons 2017 and 2018, which warrants further monitoring (possibly distinguishing between wet and dry deposition).

With respect to rainwater harvesting efforts, the mostly low EC values obtained for the Dhofar mountains stations are considered generally beneficial. However, if the gathered water is supposed to be used as drinking water, the partly elevated PO_4^{3-} and NH_4^+ concentrations may be of concern. While we ignored these values in the present study, because they probably represent artefacts (e.g., bird droppings), these very contaminations may be practically relevant in a rainwater harvesting context, warranting microbiological analyses.

Finally, we emphasize that the applied methodological framework, combining automatic bulk precipitation sampling along elevation gradients from the coast to the hinterland and air mass back-trajectory modeling, is transferable and can help to study atmospheric element cycling and deposition in other regions.

Declaration of Competing Interest

The authors declare that they have no known competing financial interests or personal relationships that could have appeared to influence the work reported in this paper.

Acknowledgments

This work was supported by the project “Submarine Groundwater Discharge: Adaption of an Autonomous Aquatic Vehicle for Robotic Measurements, Sampling and Monitoring”, funded by The Research Council of Oman (TRC Research Contract No. TRC/RCP/15/001). Further funding was received from the SMART Project through the Helmholtz European Partnering Initiative (Project ID Number PIE-0004). Moreover, we thank the staff of the Ministry of Regional Municipalities and Water Resources of Oman for their continuous support. We also gratefully acknowledge the NOAA Air Resources Laboratory (ARL) for the provision of the HYSPLIT transport and dispersion model (https://www.ready.noaa.gov/HYSPLIT.php) used in this publication. Finally, we are thankful for the insightful and constructive reviewer comments that improved the manuscript.

Appendix A. Supplementary data

Supplementary data 1 (Tables S1 and S2, Figures S1-S5)

Supplementary data 2 (Table S3, Excel file)

Data availability

Hydrochemical and meta data can be found in the Supplementary Material of this article.

References

Abdalla, O.A.E., Al-Hosni, T., Al-Rawahi, A., Kacimov, A., Clark, I., 2018. Coupling isotopic and piezometric data to infer groundwater recharge mechanisms in arid areas: example of Samail Catchment, Oman. Hydrogeology Journal 26(8), 2561–2573. https://doi.org/10.1007/s10040-018-1818-y

Abdul-Wahab, S.A., 2003. Analysis of thermal inversions in the Khareef Salalah region in the Sultanate of Oman. Journal of Geophysical Research: Atmospheres 108(D9), 4274. https://doi.org/10.1029/2002jd003083

Abdul-Wahab, S.A., Al-Damkhi, A.M., Al-Hinai, H., Al-Najar, K.A., Al-Kalbani, M.S., 2010. Total fog and rainwater collection in the Dhofar region of the Sultanate of Oman during the monsoon season. Water International 35(1), 100–109. https://doi.org/10.1080/02508060903502984

Abdul-Wahab, S.A., Al-Hinai, H., Al-Najar, K.A., Al-Kalbani, M.S., 2007. Feasibility of fog water collection: a case study from Oman. Journal of Water Supply: Research and Technology-Aqua 56(4), 275–280. https://doi.org/10.2166/aqua.2007.045

Abdul-Wahab, S.A., Worthing, M.A., Al-Maamari, S., 2005. Mineralogy of atmospheric suspended dust in three indoor and one outdoor location in Oman. Environmental Monitoring and Assessment 107(1–3), 313–327. https://doi.org/10.1007/s10661-005-3112-4

Ahmed, A.F.M., Singh, R.P., Elmubarak, A.H., 1990. Chemistry of atmospheric precipitation at the Western Arabian Gulf Coast. Atmospheric Environment. Part A. General Topics 24(12), 2927–2934. https://doi.org/10.1016/0960-1686(90)90473-z

Alabdula'aly, A.I., Khan, M.A., 2000. Chemistry of rain water in Riyadh, Saudi Arabia. Archives of Environmental Contamination and Toxicology 39(1), 66–73. https://doi.org/10.1007/s002440010081

491 Alcalá, F.J., Custodio, E., 2008. Atmospheric chloride deposition in continental Spain. Hydrological
492 Processes 22(18), 3636–3650. https://doi.org/10.1002/hyp.6965

493 Al-Shidi, H.K., Sulaiman, H., Alrubkhi, S.M., 2020. Mass concentration and morphological analysis of
494 PM10 and PM2.5 particles in congested roads during day hours in three major cities of
495 Oman. International Journal of Environmental Health Research 32(4), 738–751.
496 https://doi.org/10.1080/09603123.2020.1795087

497 Anoop, T.R., Kumar, V.S., Shanas, P.R., Johnson, G., 2015. Surface wave climatology and its variability
498 in the North Indian Ocean based on ERA-Interim reanalysis. Journal of Atmospheric and
499 Oceanic Technology 32(7), 1372–1385. https://doi.org/10.1175/jtech-d-14-00212.1

500 Appelo, C.A.J., Postma, D., 2004. Geochemistry, groundwater and pollution. Leiden, The Netherlands:
501 Balkema Publishers.

502 Askri, B., Ahmed, A.T., Al-Shanfari, R.A., Bouhlila, R., Al-Farisi, K.B.K., 2016. Isotopic and geochemical
503 identifications of groundwater salinisation processes in Salalah coastal plain, Sultanate of
504 Oman. Geochemistry 76(2), 243–255. https://doi.org/10.1016/j.chemer.2015.12.002

505 Asman, W.A.H., Ridder, T.B., Reijnders, H.F.R., Slanina, J., 1982. Influence and prevention of bird-
506 droppings in precipitation chemistry experiments. Water, Air, and Soil Pollution 17(4), 415–
507 420. https://doi.org/10.1007/bf00460108

508 Blew, R.D., Edmonds, R.L., 1995. Precipitation Chemistry along an Inland Transect on the Olympic
509 Peninsula, Washington. Journal of Environmental Quality 24(2), 239–245.
510 https://doi.org/10.2134/jeq1995.00472425002400020005x

511 Bresciani, E., Ordens, C.M., Werner, A.D., Batelaan, O., Guan, H., Post, V.E.A., 2014. Spatial variability
512 of chloride deposition in a vegetated coastal area: Implications for groundwater recharge
513 estimation. Journal of Hydrology 519, 1177–1191.
514 https://doi.org/10.1016/j.jhydrol.2014.08.050

515 Bruno, M.F., Molfetta, M.G., Totaro, V., Mossa, M., 2020. Performance assessment of ERA5 Wave
516 data in a swell dominated region. Journal of Marine Science and Engineering 8(3), 214.
517 https://doi.org/10.3390/jmse8030214

518 Carroll, D., 1962. Rainwater as a chemical agent of geologic processes – A review. Geological Survey
519 Water-Supply Paper 1535-G. US Geological Survey.

520 Cartwright, I., Gilfedder, B., Hofmann, H., 2013. Transient hydrological conditions implied by chloride
521 mass balance in southeast Australian rivers. Chemical Geology 357, 29–40.
522 https://doi.org/10.1016/j.chemgeo.2013.08.028

Cartwright, I., Hofmann, H., Currell, M. J., Fifield, L.K., 2017. Decoupling of solutes and water in regional groundwater systems: The Murray Basin, Australia. Chemical Geology 466, 466–478. https://doi.org/10.1016/j.chemgeo.2017.06.035

Cartwright, I., Weaver, T.R., Fifield, L.K., 2006. Cl/Br ratios and environmental isotopes as indicators of recharge variability and groundwater flow: An example from the southeast Murray Basin, Australia. Chemical Geology 231(1–2), 38–56. https://doi.org/10.1016/j.chemgeo.2005.12.009

Charabi, Y., Abdul-Wahab, S., Al-Rawas, G., Al-Wardy, M., Fadlallah, S., 2018. Investigating the impact of monsoon season on the dispersion of pollutants emitted from vehicles: A case study of Salalah City, Sultanate of Oman. Transportation Research Part D: Transport and Environment 59, 108–120. https://doi.org/10.1016/j.trd.2017.12.019

Christofi, C., Bruggeman, A., Kuells, C., Constantinou, C., 2020. Hydrochemical evolution of groundwater in gabbro of the Troodos Fractured Aquifer. A comprehensive approach. Applied Geochemistry 114, 104524. https://doi.org/10.1016/j.apgeochem.2020.104524

Davies, P.J., Crosbie, R.S., 2018. Mapping the spatial distribution of chloride deposition across Australia. Journal of Hydrology 561, 76–88. https://doi.org/10.1016/j.jhydrol.2018.03.051

Davis, S.N., Whittemore, D.O., Fabryka-Martin, J., 1998. Uses of chloride/bromide ratios in studies of potable water. Ground Water 36(2), 338–350. https://doi.org/10.1111/j.1745-6584.1998.tb01099.x

Decina, S.M., Hutyra, L.R., Templer, P.H., 2019. Hotspots of nitrogen deposition in the world's urban areas: a global data synthesis. Frontiers in Ecology and the Environment 18(2), 92–100. https://doi.org/10.1002/fee.2143

Duce, R.A., Hoffman, G.L., Zoller, W.H., 1975. Atmospheric trace metals at remote northern and southern hemisphere sites: pollution or natural? Science 187(4171), 59–61. https://doi.org/10.1126/science.187.4171.59

Edmunds, W.M., 2010. Conceptual models for recharge sequences in arid and semi-arid regions using isotopic and geochemical methods. In: Wheater, H.S., Mathias, S.A., Li, X. (eds.), Groundwater Modelling in Arid and Semi-arid Areas. Cambridge University Press, Cambridge, 21–37.

Engelbrecht, J.P., Stenchikov, G., Prakash, P.J., Lersch, T., Anisimov, A., Shevchenko, I., 2017. Physical and chemical properties of deposited airborne particulates over the Arabian Red Sea coastal plain. Atmospheric Chemistry and Physics 17(18), 11467–11490. https://doi.org/10.5194/acp-17-11467-2017

Erickson, D.J., Ghan, S.J., Penner, J.E., 1990. Global ocean-to-atmosphere dimethyl sulfide flux. Journal of Geophysical Research 95(D6), 7543–7552. https://doi.org/10.1029/jd095id06p07543

Friesen, J., Zink, M., Bawain, A., Müller, T., 2018. Hydrometeorology of the Dhofar cloud forest and its implications for groundwater recharge. Journal of Hydrology: Regional Studies 16, 54–66. https://doi.org/10.1016/j.ejrh.2018.03.002

Guan, H., Love, A.J., Simmons, C.T., Makhnin, O., Kayaalp, A.S., 2010. Factors influencing chloride deposition in a coastal hilly area and application to chloride deposition mapping. Hydrology and Earth System Sciences 14(5), 801–813. https://doi.org/10.5194/hess-14-801-2010

Hildebrandt, A., Al Aufi, M., Amerjeed, M., Shammas, M., Eltahir, E.A.B., 2007. Ecohydrology of a seasonal cloud forest in Dhofar: 1. Field experiment. Water Resources Research 43(10), W10411. https://doi.org/10.1029/2006wr005261

Hussain, M., Al-Shaibani, A., Al-Ramadan, K., Wood, W.W., 2020. Geochemistry and isotopic analysis of brines in the coastal sabkhas, Eastern region, Kingdom of Saudi Arabia. Journal of Arid Environments 178, 104142. https://doi.org/10.1016/j.jaridenv.2020.104142

IEM, 2021. Iowa Environmental Mesonet. Iowa State University. https://mesonet.agron.iastate.edu/request/download.phtml?network=OM__ASOS (last access on 5 October 2021).

Imes, J.L., Wood, W.W., 2007. Solute and isotope constraint of groundwater recharge simulation in an arid environment, Abu Dhabi Emirate, United Arab Emirates. Hydrogeology Journal 15(7), 1307–1315. https://doi.org/10.1007/s10040-007-0177-x

Javed, W., Wubulikasimu, Y., Figgis, B., Guo, B., 2017. Characterization of dust accumulated on photovoltaic panels in Doha, Qatar. Solar Energy 142, 123–135. https://doi.org/10.1016/j.solener.2016.11.053

Johansen, A.M., Siefert, R.L., Hoffmann, M.R., 1999. Chemical characterization of ambient aerosol collected during the southwest monsoon and intermonsoon seasons over the Arabian Sea: Anions and cations. Journal of Geophysical Research: Atmospheres 104(D21), 26325–26347. https://doi.org/10.1029/1999jd900405

Junge, C.E., Werby, R.T., 1958. The concentration of chloride, sodium, potassium, calcium, and sulfate in rain water over the United States. Journal of Meteorology 15(5), 417–425. https://doi.org/10.1175/1520-0469(1958)015<0417:tcocsp>2.0.co;2

Keene, W.C., Maring, H., Maben, J.R., Kieber, D.J., Pszenny, A.A.P., Dahl, E.E., Izaguirre, M.A., Davis, A.J., Long, M.S., Zhou, X., Smoydzin, L., Sander, R., 2007. Chemical and physical characteristics of nascent aerosols produced by bursting bubbles at a model air-sea interface. Journal of Geophysical Research 112, D21202. https://doi.org/10.1029/2007jd008464

Keppel, M.N., Post, V.E.A., Love, A.J., Clarke, J.D.A., Werner, A.D., 2012. Influences on the carbonate hydrochemistry of mound spring environments, Lake Eyre South region, South Australia. Chemical Geology 296–297, 50–65. https://doi.org/10.1016/j.chemgeo.2011.12.017

Khalaf, F.I., Al-Kadi, A., Al-Saleh, S., 1985. Mineralogical composition and potential sources of dust fallout deposits in Kuwait, Northern Arabian Gulf. Sedimentary Geology 42(3–4), 255–278. https://doi.org/10.1016/0037-0738(85)90047-8

Ladouche, B., Luc, A., Nathalie, D., 2009. Chemical and isotopic investigation of rainwater in Southern France (1996–2002): Potential use as input signal for karst functioning investigation. Journal of Hydrology 367(1–2), 150–164. https://doi.org/10.1016/j.jhydrol.2009.01.012

Liotta, M., Martínez Cruz, M., Ferrufino, A., Rüdiger, J., Gutmann, A., Rojas Cerda, K.V., Bobrowski, N., de Moor, J.M., 2021. Magmatic signature in acid rain at Masaya volcano, Nicaragua: Inferences on element volatility during lava lake degassing. Chemical Geology 585, 120562. https://doi.org/10.1016/j.chemgeo.2021.120562

Matter, J.M., Waber, H.N., Loew, S., Matter, A., 2005. Recharge areas and geochemical evolution of groundwater in an alluvial aquifer system in the Sultanate of Oman. Hydrogeology Journal 14(1–2), 203–224. https://doi.org/10.1007/s10040-004-0425-2

Macumber, P.G., Al Abri, R., Al Akhzami, S., 1998. Hydrochemical facies in the groundwater of central and southern Oman. In: Alsharan, A. S., Glennie, K. W., Whittle, G. L., Kendall, C. G. St. C. (eds.). Quaternary Deserts and Climatic Change. Balkema, Rotterdam, 511–520.

Michelsen, N., Laube, G., Friesen, J., Weise, S.M., Bait Said, A.B.A., Müller, T., 2019. Technical note: A microcontroller-based automatic rain sampler for stable isotope studies. Hydrology and Earth System Sciences 23(6), 2637–2645. https://doi.org/10.5194/hess-23-2637-2019

Michelsen, N., Reshid, M., Siebert, C., Schulz, S., Knöller, K., Weise, S. M., Rausch, R., Al-Saud, M., Schüth, C., 2015. Isotopic and chemical composition of precipitation in Riyadh, Saudi Arabia. Chemical Geology 413, 51–62. https://doi.org/10.1016/j.chemgeo.2015.08.001

Michelsen, N., van Geldern, R., Roßmann, Y., Bauer, I., Schulz, S., Barth, J.A.C., Schüth, C., 2018. Comparison of precipitation collectors used in isotope hydrology. Chemical Geology 488, 171–179. https://doi.org/10.1016/j.chemgeo.2018.04.032

Ministry of Petroleum and Minerals, 1998. Salalah, Geological Map. Sheet NE40-9D, Ministry of Petroleum and Minerals, Sultanate of Oman.

Müller, T., Friesen, J., Weise, S.M., Al Abri, O., Bait Said, A.B.A., Michelsen, N., 2020. Stable isotope composition of Cyclone Mekunu rainfall, Southern Oman. Water Resources Research 56(12), e2020WR027644. https://doi.org/10.1029/2020wr027644

Nothaft, D.B., Templeton, A.S., Boyd, E.S., Matter, J.M., Stute, M., Paukert Vankeuren, A.N., 2021. Aqueous geochemical and microbial variation across discrete depth intervals in a peridotite aquifer assessed using a packer system in the Samail Ophiolite, Oman. Journal of Geophysical Research: Biogeosciences 126(9), e2020JB020756. https://doi.org/10.1029/2021jg006319

Paukert, A.N., Matter, J.M., Kelemen, P.B., Shock, E.L., Havig, J.R., 2012. Reaction path modeling of enhanced *in situ* CO_2 mineralization for carbon sequestration in the peridotite of the Samail Ophiolite, Sultanate of Oman. Chemical Geology 330–331, 86–100. https://doi.org/10.1016/j.chemgeo.2012.08.013

Pósfai, M., Axisa, D., Tompa, É., Freney, E., Bruintjes, R., Buseck, P.R., 2013. Interactions of mineral dust with pollution and clouds: An individual-particle TEM study of atmospheric aerosol from Saudi Arabia. Atmospheric Research 122, 347–361. https://doi.org/10.1016/j.atmosres.2012.12.001

Riechelmann, D.F.C., Riechelmann, S., Schröder-Ritzrau, A., 2022. Long-term elemental trends in drip waters from monitoring Bunker Cave: New insights for past precipitation variability. Chemical Geology 590, 120704. https://doi.org/10.1016/j.chemgeo.2021.120704

Rolph, G., Stein, A., Stunder, B., 2017. Real-time Environmental Applications and Display sYstem: READY. Environmental Modelling & Software 95, 210–228. https://doi.org/10.1016/j.envsoft.2017.06.025

Salter, M.E., Hamacher-Barth, E., Leck, C., Werner, J., Johnson, C.M., Riipinen, I., Nilsson, E.D., Zieger, P., 2016. Calcium enrichment in sea spray aerosol particles. Geophysical Research Letters 43, 8277–8285. https://doi.org/10.1002/2016gl070275

Sanz, M.J., Carratalá, A., Gimeno, C., Millán, M.M., 2002. Atmospheric nitrogen deposition on the east coast of Spain: relevance of dry deposition in semi-arid Mediterranean regions. Environmental Pollution 118(2), 259–272. https://doi.org/10.1016/s0269-7491(01)00318-9

Savoie, D.L., Prospero, J.M., Nees, R.T., 1987. Nitrate, non-sea-salt sulfate, and mineral aerosol over the northwestern Indian Ocean. Journal of Geophysical Research 92(D1), 933–942. https://doi.org/10.1029/jd092id01p00933

651 Scanlon, B.R., Healy, R.W., Cook, P.G., 2002. Choosing appropriate techniques for quantifying
652 groundwater recharge. Hydrogeology Journal 10(1), 18–39. https://doi.org/10.1007/s10040-
653 001-0176-2

654 Scanlon, B.R., Keese, K.E., Flint, A.L., Flint, L.E., Gaye, C.B., Edmunds, W.M., Simmers, I., 2006. Global
655 synthesis of groundwater recharge in semiarid and arid regions. Hydrological Processes
656 20(15), 3335–3370. https://doi.org/10.1002/hyp.6335

657 Schulz, S., Horovitz, M., Rausch, R., Michelsen, N., Mallast, U., Köhne, M., Siebert, C., Schüth, C., Al-
658 Saud, M., Merz, R., 2015. Groundwater evaporation from salt pans: Examples from the
659 eastern Arabian Peninsula. Journal of Hydrology 531, 792–801.
660 https://doi.org/10.1016/j.jhydrol.2015.10.048

661 Schemenauer, R.S., Cereceda, P., 1992. Monsoon cloudwater chemistry on the Arabian Peninsula.
662 Atmospheric Environment. Part A. General Topics 26(9), 1583–1587.
663 https://doi.org/10.1016/0960-1686(92)90058-s

664 Semeniuk, T.A., Bruintjes, R.T., Salazar, V., Breed, D.W., Jensen, T.L., Buseck, P.R., 2014. Individual
665 aerosol particles in ambient and updraft conditions below convective cloud bases in the
666 Oman mountain region. Journal of Geophysical Research: Atmospheres 119(5), 2511–2528.
667 https://doi.org/10.1002/2013jd021165

668 Shammas, M.I., Jacks, G., 2007. Seawater intrusion in the Salalah plain aquifer, Oman. Environmental
669 Geology 53(3), 575–587. https://doi.org/10.1007/s00254-007-0673-2

670 Solder, J.E., Jurgens, B.C., 2020. Evaluation of soil zone processes and a novel radiocarbon correction
671 approach for groundwater with mixed sources. Journal of Hydrology 588, 124766.
672 https://doi.org/10.1016/j.jhydrol.2020.124766

673 Stein, A.F., Draxler, R.R., Rolph, G.D., Stunder, B.J.B., Cohen, M.D., Ngan, F., 2015. NOAA's HYSPLIT
674 Atmospheric Transport and Dispersion Modeling System. Bulletin of the American
675 Meteorological Society 96(12), 2059–2077. https://doi.org/10.1175/bams-d-14-00110.1

676 Strauch, G., Al-Mashaikhi, K.S., Bawain, A., Knöller, K., Friesen, J., Müller, T., 2014. Stable H and O
677 isotope variations reveal sources of recharge in Dhofar, Sultanate of Oman. Isotopes in
678 Environmental and Health Studies 50(4), 475–490.
679 https://doi.org/10.1080/10256016.2014.961451

680 Tso, C.H.M., Monteith, D., Scott, T., Watson, H., Dodd, B., Pereira, M.G., Henrys, P., Hollaway, M.,
681 Rennie, S., Lowther, A., Watkins, J., Killick, R., Blair, G.,2022. The evolving role of weather
682 types on rainfall chemistry under large reductions in pollutant emissions. Environmental
683 Pollution 299, 118905. https://doi.org/10.1016/j.envpol.2022.118905

Vet, R., Artz, R.S., Carou, S., Shaw, M., Ro, C.-U., Aas, W., Baker, A., Bowersox, V.C., Dentener, F., Galy-Lacaux, C., Hou, A., Pienaar, J.J., Gillett, R., Forti, M.C., Gromov, S., Hara, H., Khodzher, T., Mahowald, N.M., Nickovic, S., Rao, P.S.P., Reid, N.W., 2014. A global assessment of precipitation chemistry and deposition of sulfur, nitrogen, sea salt, base cations, organic acids, acidity and pH, and phosphorus. Atmospheric Environment 93, 3–100. https://doi.org/10.1016/j.atmosenv.2013.10.060

Wang, W.-L., Song, G., Primeau, F., Saltzman, E.S., Bell, T.G., Moore, J.K., 2020. Global ocean dimethyl sulfide climatology estimated from observations and an artificial neural network. Biogeosciences 17(21), 5335–5354. https://doi.org/10.5194/bg-17-5335-2020

Weijers, E.P., Vugts, H.F., 1990. The composition of bulk precipitation on a coastal island with agriculture compared to an urban region. Atmospheric Environment 24(12), 3021–3031. https://doi.org/10.1016/0960-1686(90)90481-2

Weyhenmeyer, C., 2000. Origin and evolution of groundwaters in the alluvial aquifer of the Eastern Batinah Coastal Plain, Sultanate of Oman. PhD Thesis, University of Bern, Switzerland.

Weyhenmeyer, C.E., Burns, S.J., Waber, H.N., Macumber, P.G., Matter, A., 2002. Isotope study of moisture sources, recharge areas, and groundwater flow paths within the eastern Batinah coastal plain, Sultanate of Oman. Water Resources Research 38(10), 1184. https://doi.org/10.1029/2000wr000149

Wood, W.W., Clark, D., Imes, J.L., Councell, T.B., 2010. Eolian Transport of Geogenic Hexavalent Chromium to Ground Water. Ground Water 48(1), 19–29. https://doi.org/10.1111/j.1745-6584.2009.00592.x

Yigiterhan, O., Alfoldy, B.Z., Giamberini, M., Turner, J.C., Al-Ansari, E.S., Abdel-Moati, M.A., Al-Maslamani, I.A., Kotb, M.M., Elobaid, E.A., Hassan, H.M., Obbard, J.P., Murray, J.W., 2018. Geochemical composition of aeolian dust and surface deposits from the Qatar Peninsula. Chemical Geology 476, 24–45. https://doi.org/10.1016/j.chemgeo.2017.10.030